Examples of applications of the peridynamic theory to the solution of static equilibrium problems

M. Zaccariotto
mirco.zaccariotto@unipd.it
F. Luongo, G. Sarego and U. Galvanetto
Department of Industrial Engineering
University of Padova
Padova
Italy

Centre of Studies and Activities for Space (CISAS)
Padova
Italy

ABSTRACT

Peridynamics is a recently proposed continuum theory based on a non local approach and formulated with integral equations. The theory is suitable for dealing with crack propagation in solid materials. The original peridynamic formulation regarded dynamic problems and was adapted to the static case mainly using a relaxation method by introducing a substantial amount of numerical damping in the time integration. In the present work the implementation of the theory within an implicit code for static crack propagation phenomena based on the Newton-Raphson method is presented and applied to several examples of static crack propagation equilibrium problems. Results obtained with the newly developed procedure are presented for various structural configurations, with different boundary and load conditions and quantitatively compared to published data.

Paper No. 4156. Manuscript received 21 February 2014, revised version received 15 September 2014, accepted 3 October 2014.

https://doi.org/10.1017/S0001924000010770 Published online by Cambridge University Press

NOMENCLATURE

a length of the crack
$\mathbf{b}$ external prescribed force vector
c bond stiffness
c_w weakened bond stiffness
d single bond weakening factor
dV_j infinitesimal volume associate to node j
E Young's modulus
$\mathbf{f}$ pairwise force function vector between two nodes
G_{Ic} elastic fracture energy release rate for mode I fracture
G_0 energy required to start the damaging process
H_i horizon sphere volume associated to node i
k_r ratio
n number of nodes
n_x number of nodes in x direction
n_y number of nodes in y direction
s bond stretch
s_c failure bond stretch
s_{max} historical maximum stretch reached by a bond
s_o peak force stretch
$\mathbf{u}$ displacement vector of node i
$\mathbf{u}_i$ acceleration vector of node i
$\mathbf{x}_i$ position vector of node
β volume reduction factor
δ horizon
Δx grid spacing
$\boldsymbol{\eta}$ current relative displacement vector
$\mu(\boldsymbol{\xi})$ history-dependent scalar damage function
v Poisson's ratio
$\boldsymbol{\xi}$ initial relative position vector
ρ density
φ damage index

1.0 INTRODUCTION

Crack propagation in solid bodies is an important problem regarding many practical applications[1]. Most methods based on classical continuum mechanics are formulated in terms of partial differential equations and require ad hoc techniques to be applied in the presence of discontinuities.

https://doi.org/10.1017/S0001924000010770 Published online by Cambridge University Press

In the last thirty years several approaches have been proposed to deal with discontinuities in structural materials, such as interface elements coupled with Cohesive Zone Models (CZM)[2-4] and the extended finite element method (XFEM)[5,6] among the most popular and successful ones. However, interface elements can only be applied if the path of the discontinuity is known a priori and it is limited to the element boundaries. Some of the drawbacks of interface elements have been overcome by the XFEM, but its extension to 3D problems appears to be rather complex[7].

In the last years, also meshless methods have been employed to study the evolution of the crack front. Several formulations and techniques are available in literature, as reviewed in[8]. In this area, many efforts have been oriented towards the extended element-free Galerkin method[9,10] and towards getting an accurate evaluation of stress intensity factor[11,12]. Peridynamics is an integral theory well suited to model crack propagation and impact analysis[13] based on a mesh-free approach as well. Since the presence of cracks in a solid represents a discontinuity in the displacement field, the peridynamic formulation, which uses only integrals, overcomes the problems of the classical continuum theory of solid mechanics. In particular, the main advantage of Peridynamics is that no *a-priori* knowledge about the crack initiation and propagation is required since the crack is free to arise and grow in every part of the structure, only according to physical and geometrical constraints[14].

In its original formulation[13], Peridynamics has been developed and applied to solve dynamic problems dealing with fast crack propagations in materials under blast or impact loadings. However, its flexibility in describing crack propagation can find useful application to static problems as well. In the previous works, Peridynamics has been applied to static conditions in a damped relaxation formulation[15] which does not appear to be very efficient from a computational point of view. To the authors' knowledge, the present study is one of the first works to describe the implementation of an equilibrium formulation employing an implicit solver for the peridynamic equations and to apply it to cases of 'quasi-static' crack propagation. Other works using a Newton-Raphson implicit approach are seen in Refs 16-18 where an implicit time integration algorithm was presented and successfully applied to a single bond. Moreover it is possible to find in the literature other implementations similar to the one presented in Ref. 19, where the authors focus their attention on the plastic behavior of the analysed material considering both similarities and differences with the classic continuum material behavior. In Ref. 21 a Newton-Raphson method is employed in order to find an equilibrium solution which could link classical FE sub-regions and peridynamic regions. At last in Ref. 20 an implicit implementation of non-ordinary state-based peridynamics for stationary crack problems is presented.

In this work, a particular emphasis is put, for the first time, on a variety of analysed cases for which a quantitative comparison with experimental or analytical data[22] is carried out. These analyses are both linear, in order to estimate the error due to the discretisation in comparison with a FEM solution, and nonlinear to illustrate the potentiality of the peridynamic approach.

The paper begins with a brief introduction to the fundamentals of Peridynamics in Section 2 and continues with a description of the relevant nonlinearity in Section 3. The results are presented in Section 4, for linear cases, and Section 5, for nonlinear problems. Conclusions were drawn in Section 6.

2.0 STATIC FORMULATION

The main assumption of Peridynamics is that the body is composed of material points which interact with other points within a finite distance named horizon, usually indicated with the Greek letter δ The interaction is called bond. In this paper, the bond-based assumption[13], which considers the

https://doi.org/10.1017/S0001924000010770 Published online by Cambridge University Press

behavior of a bond completely independent of all the others, is made. The equation that controls the motion of the points of the structure assumes the following form:

$$\rho\ddot{\mathbf{u}}_i = \int_{H_i} \mathbf{f}\left[\mathbf{u}(\mathbf{x}_j,t)-\mathbf{u}(\mathbf{x}_i,t),\mathbf{x}_j-\mathbf{x}_i\right]dV_j + \mathbf{b}(\mathbf{x}_i,t) \qquad \forall \mathbf{x}_j \in H_i \qquad \ldots (1)$$

where H_i is the spherical region of radius δ centred at point $\mathbf{x}_i$ (see Fig. 1), **u** is the displacement vector field, **b** is a body density force vector and **f** is called pairwise force function, which is a force per unit square volume that represents the force that point $\mathbf{x}_j$ exerts on point $\mathbf{x}_i$.

Force **f** acts along the line connecting the two points, therefore it does not produce any moment on them. Under this assumption, and naming:

$$\begin{aligned}\xi &= \mathbf{x}_j - \mathbf{x}_i \\ \eta &= \mathbf{u}(\mathbf{x}_i,t)-\mathbf{u}(\mathbf{x}_j,t)\end{aligned} \qquad \ldots (2)$$

the initial relative position and the current relative displacement respectively, the stretch of the bond can be expressed by the following formula:

$$s = \frac{|\boldsymbol{\eta}+\xi| - |\xi|}{|\xi|} \qquad \ldots (3)$$

In the prototype microelastic brittle material (PMB) proposed in Ref. 13, the stretch and the pairwise force function **f** are related according to Equation (4):

$$\mathbf{f} = c\cdot s\cdot \mu(\xi)\cdot\frac{\boldsymbol{\eta}+\xi}{|\boldsymbol{\eta}+\xi|} \cong c\cdot s\cdot\mu(\xi)\cdot\frac{\xi}{|\xi|} \qquad \ldots (4)$$

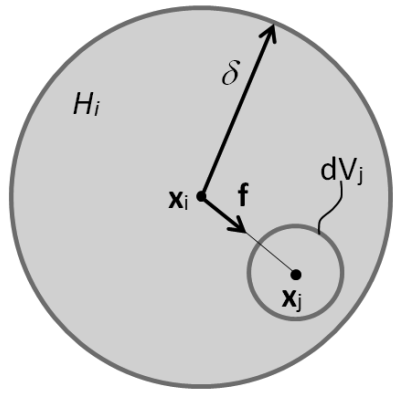


Figure 1. Material point $\mathbf{x}_j$ interacts by means of peridynamic forces with all points within a spherical neighborhood of radius δ. Every material point $\mathbf{x}_j$ is associated to a volume dV_j and exerts a force **f** on material point $\mathbf{x}_i$.

https://doi.org/10.1017/S0001924000010770 Published online by Cambridge University Press

where c is the bond stiffness, $\mu(\xi)$ is a history-dependent scalar function which takes the values 1 or 0 depending on the bond status: 1 identifies an active bond, while 0 means that the bond is broken. The second part of Equation (4) is used when the 'small displacement' approximation is made. Considerations regarding the elastic deformation energy allow the definition of the bond stiffness c in terms of the Young's modulus E and of the horizon radius δ. The bond stiffness c takes the form reported in Equation (5) for the 3D case and the forms given in Equation (6) for the plane state cases (see Ref. 13)).

$$c = \frac{12 \cdot E}{\pi \cdot \delta^4} \quad \text{for 3D case} \qquad \ldots (5)$$

$$\begin{aligned} c &= \frac{9 \cdot E}{\pi \cdot t \cdot \delta^3} \quad \text{plane stress} \\ c &= \frac{48 \cdot E}{5 \cdot \pi \cdot t \cdot \delta^3} \quad \text{plane strain} \end{aligned} \qquad \ldots (6)$$

As a consequence of the peridynamic bond-based formulation, the value of the Poisson's ratio in the 3D and plane strain cases is constrained to $\nu = 0{\cdot}25$, while as for the plane stress it is restricted to $\nu = 0{\cdot}33$. This limitation has been removed with the state-based formulation of the theory presented in Refs 14 and 23.

The numerical approximation of the peridynamic equation starts with the sub-division of the structure into nodes: each node is associated to a certain volume and the union of all volumes covers the entire volume of the body.
Therefore, the discretised form of the Equation (1) is:

$$\begin{aligned} &\rho \ddot{\mathbf{u}}_i^n = \sum_j \mathbf{f}(\mathbf{u}_j^n - \mathbf{u}_i^n, \mathbf{x}_j - \mathbf{x}_i)\beta \Delta V_j + \mathbf{b}_i^n \\ &\forall j \in H_i \end{aligned} \qquad \ldots (7)$$

where i is the index of the central node, also called source node, and it is fixed in Equation (7), j is the family node index and represents all nodes within the horizon of node i, n is the time step number, ΔV_j is the discretised volume associated to node j (see Fig. 1) and β is the volume reduction factor, that is a coefficient which takes into consideration that the volume of nodes near the horizon spherical surface are partially inside H_i and it is calculated as defined in Ref. 24. Loads and boundary conditions should be applied not only to surface nodes, but also to internal nodes, within a horizon thickness of the external surface[13,25]. This consideration respects the nature of the peridynamic equation itself, which involves force per unit volume (densities) as a natural boundary condition. For the purposes of this paper, the time dependence is removed from Equation (7), and the first term is set equal to zero, since the problem can be studied as a sequence of static analyses with incremental external load or displacement. The equation solved in the present paper is therefore Equation (8):

$$\begin{aligned} &\sum_j \mathbf{f}(\mathbf{u}_j^n - \mathbf{u}_i^n, \mathbf{x}_j - \mathbf{x}_i)\beta \Delta V_j + \mathbf{b}_i^n = 0 \\ &\forall j \in H_i \end{aligned} \qquad \ldots (8)$$

https://doi.org/10.1017/S0001924000010770 Published online by Cambridge University Press

In Equation (8) n is the load step, moreover the small displacement assumption is made, so that the pairwise force **f** is defined as in the second part of Equation (4).

3.0 NONLINEARITY

In the prototype microelastic brittle material proposed in Ref. 25, the stretch s and the value (positive for traction and negative for compression) of the pairwise force function **f** are related according to Equation (4) and such relation is shown in Fig. 2(a). When a bond is broken, it is removed from the computations so that the stiffness matrix of the whole structure changes and the problem becomes nonlinear. In this paper the material adopted to model each bond is characterised by a bilinear relationship between the scalar value of the pairwise force function **f** and the bond stretch s, in order to model an elastic-progressively damaging material (see Fig. 2(b)):

$$\mathrm{f}(s)=\begin{cases} c\cdot s & s\le s_0 & \text{Undamaged state} \\ c\cdot\left(1-\dfrac{s_{\max}-s_0}{s_{\max}}\cdot\dfrac{s_c}{s_c-s_0}\right)\cdot s & s<s_{\max}\ \text{ and }\ s_0<s_{\max}<s_c & \text{Unloading or reloading} \\ c\cdot\left(1-\dfrac{s-s_0}{s}\cdot\dfrac{s_c}{s_c-s_0}\right)\cdot s & s=s_{\max}\ \text{ and }\ s_0<s_{\max}<s_c & \text{Max stretch increasing loading} \\ 0 & s\ge s_c & \text{Failed bond} \end{cases} \quad \ldots (9)$$

where c is the bond stiffness previously defined, s_0 is the bond stretch at the linear elastic limit, s_c is the bond stretch at failure and s_{max} is the maximum value of the stretch in the deformation history of the bond. Similar constitutive laws have often been adopted to simulate damage in mechanics[2].

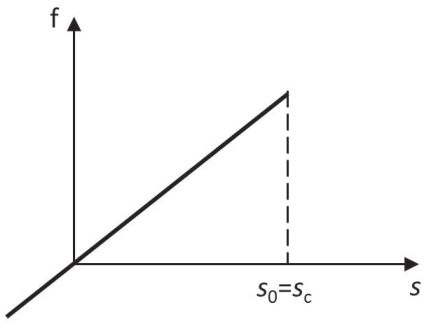
As it is possible to notice from the previous system of equations, a progressive damage formulation has been implemented: in this way, when the material overcomes the linear elastic stretch limit s_0, the irreversibility of the progressive damage is taken into account and the stiffness is reduced by introducing the term d according to Equations (10) that express the weakening of the single bond:

$$\begin{aligned} d &= \frac{s-s_0}{s}\cdot\frac{s_c}{s_c-s_0} \\ c_w &= c\cdot(1-d) \end{aligned} \quad \ldots (10)$$

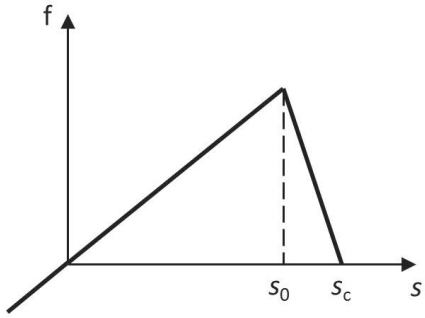
where c_w is the weakened bond stiffness. If the bond is subjected to an unloading phase after having passed the elastic limit, the slope of the line $f = f(s)$ is smaller than the initial one, as it is shown in Fig. 3: in fact, the initial slope is the pristine stiffness c while when weakened it is reduced by the term $(1 - d)$.

Moreover, a bond in compression never fails and its stiffness remains equal to the initial one whenever the stretch becomes negative. The value of s_c is estimated by evaluating the energy required to have the complete separation of the fracture surfaces during crack propagation[13]. In the peridynamic approach, this requires the evaluation of an integral, reported in Equation (11) for the case of a prototype brittle material; this integral must be estimated in a domain equal to one horizon sphere[24].

https://doi.org/10.1017/S0001924000010770 Published online by Cambridge University Press

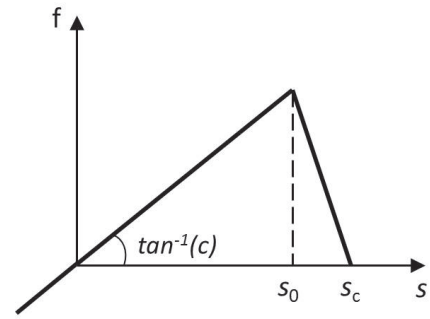


(a)

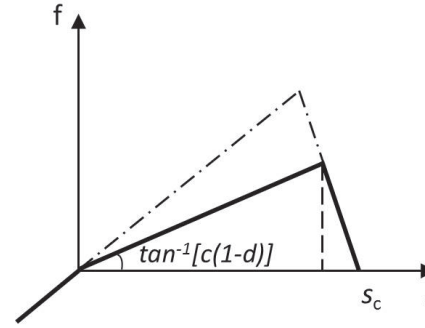


(b)

Figure 2. Bond force *f* vs bond stretch *s* law: (a) PMB material, (b) bilinear law. s_0 is the peak force stretch, while s_c is the failure bond stretch.



(a)



(b)

Figure 3. Bond force *f* vs bond stretch *s* law: (a) intact bond, (b) weakened bond. *c* is the pristine bond stiffness and *d* is the bond weakening factor defined in Equation (10).

$$G_{Ic} = \int_0^{\delta} dz \int_0^{2\pi} d\theta \int_z^{\delta} d\xi \int_0^{\cos^{-1}(z/\xi)} d\phi \frac{c s_c^2 \xi}{2} \mathrm{Sin}(\phi) \xi^2 \quad \ldots (11)$$

where G_{Ic} is the elastic fracture energy release rate for mode I fracture. Figure 4 shows the main variables used in Equation (11). The failure stretch in the case of a prototype brittle material is reported in Equation (12) and Equations (13) for the 3D and 2D cases respectively.

$$s_c = \sqrt{\frac{5G_{Ic}}{6E\delta}} \quad \text{3D case} \quad \ldots (12)$$

$$s_c = \sqrt{\frac{4\pi G_{Ic}}{9E\delta}} \quad \text{plane stress}$$

$$s_c = \sqrt{\frac{5\pi G_{Ic}}{12E\delta}} \quad \text{plane strain} \quad \ldots (13)$$

https://doi.org/10.1017/S0001924000010770 Published online by Cambridge University Press

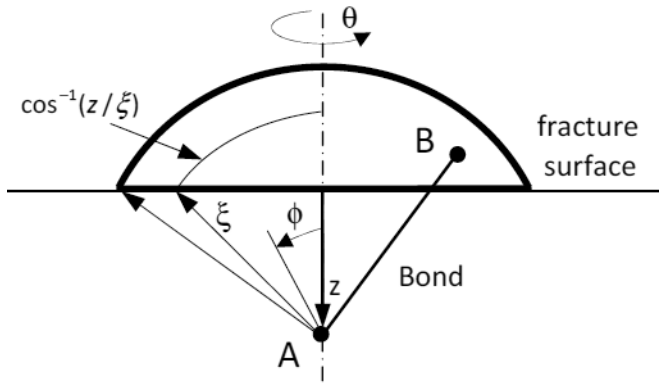


Figure 4. The failure stretch is evaluated by computing the integral of the energy required to break the bonds in order to allow the creation of a crack surface inside the solid.

Similarly, the integral of Equation (11) can be evaluated using the bilinear force function of Fig. 2(b), if the energy required to start the damaging process (i.e. the stretch reached the value s_0) is defined as G_0 and k_r is the ratio s_c/s_0, the result obtained for the plane stress case is reported in Equation (14):

$$s_0 = \sqrt{\frac{4\pi G_0}{9E\delta}} \quad \text{and} \quad k_r = \frac{s_c}{s_0} = \frac{G_{Ic}}{G_0} \qquad \ldots (14)$$

The expression of k_r in Equation (14) is general and valid for other case as well, such as 3D case and plane strain case.

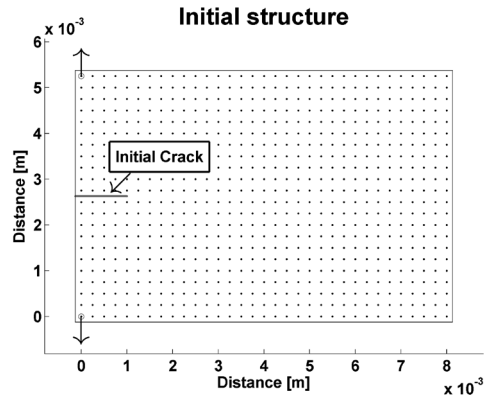
In the present section the weakening of the single bond has been mentioned as defined in Equation (10) and it is employed in the nonlinear analyses, so a brief explanation on the peridynamic concept of damage can be useful for a clear understanding. In some papers such as Ref. 25, one of the advantages of the introduction of failure at bond level is the possibility to define the notion of local damage for each point of the body. Damage index φ is defined as:

$$\varphi(\mathbf{x}_i, t) = 1 - \frac{\int_{H_i} \mu(\mathbf{x}_i, t, \xi) dV_\xi}{\int_{H_i} dV_\xi} \qquad \ldots (15)$$

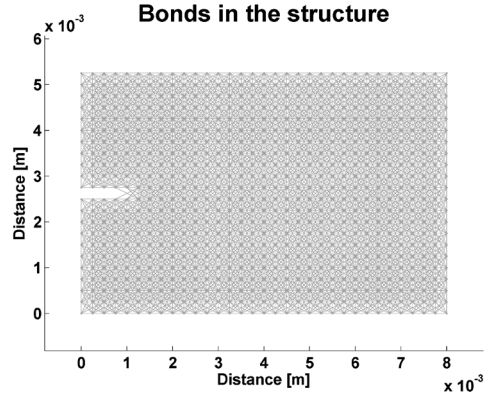
The damage index φ in a node $\mathbf{x}_i$ of the grid can be defined as the ratio of the number of broken bonds to the total number of bonds initially connected with that node. Figure 5 shows a plate with an initial crack on which a double cantilevered test is performed. The system is discretised, according to the peridynamic theory, as a set of material points, which interact through bonds: they are represented as lines in Fig. 5(b) and Fig. 5(c). Fig. 5(b) shows the crack as a zone of the plate with no bonds. Figure 5(c) is a magnified view of the cracked area where it is possible to see that no bonds intersect the initial crack.

All simulations presented in this section and in the next were performed with an in-house Matlab code in double precision.

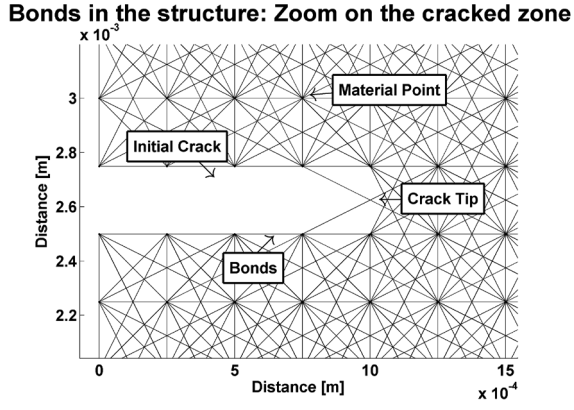
https://doi.org/10.1017/S0001924000010770 Published online by Cambridge University Press



(a)



(b)



(c)

Figure 5. (a) Initial crack on a plate subjected to a double cantilevered test; (b) bonds between the points of the discretised body; (c) zoom in the initial cracked area.

https://doi.org/10.1017/S0001924000010770 Published online by Cambridge University Press

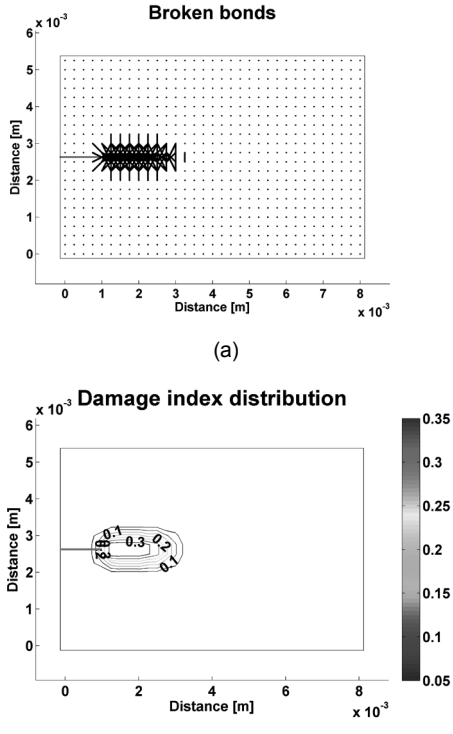


Figure 6. (a) the cracked bonds due to crack propagation phenomena; (b) the local damage index.

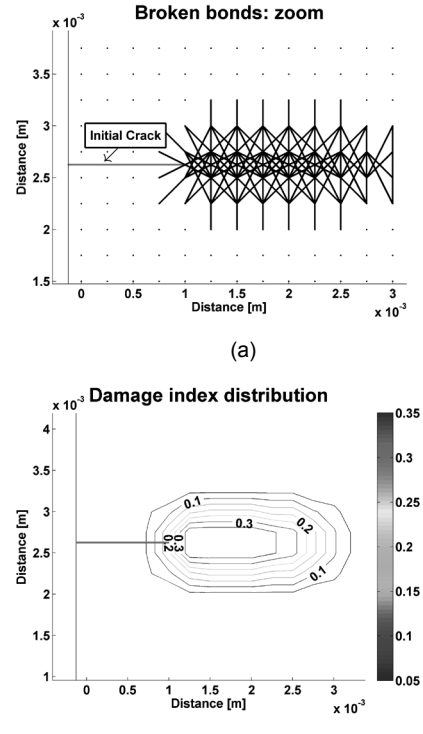


Figure 7. (a) zoom of Fig. 6(a): the highlighted bonds are broken due to crack propagation phenomena; (b) zoom of Fig. 6(b): the local damage index is displayed.

The crack propagation due to the applied load is shown in Fig. 6: in Fig. 6(a) the broken bonds are highlighted, whereas in Fig. 6(b) the local damage index is represented. In Fig. 7 a zoom of the cracked tip area after the crack propagation is shown.

In peridynamic models the crack usually separates nodes which end up being on the two different sides of the crack itself. In the case of a horizon radius equal to three times the grid spacing, the damage index can take values such as those shown in Fig. 8, which justifies the values in Fig. 6 and Fig. 7: a value $\varphi \approx 0{\cdot}4$ indicates that a crack has cut all the bonds on one side of the source node.

3.1 Newton-Raphson method

Since the constitutive law of the bonds is bilinear and the bonds can break, the stiffness of the structure is not constant and therefore the problem is nonlinear. For this reason, an iterative procedure based on the Newton-Raphson (N-R) method can be used to solve numerically the problem.

In the case under investigation, if the body is divided into n nodes that are free to move, then the system has $2n$ degrees of freedom corresponding to the horizontal and vertical displacement components for each node. The stiffness matrix has dimension $2n \times 2n$ and its i,j component contains the stiffness contributions of each bond connected to the corresponding i,j degree of freedom. As the external load increases, one or more bonds will be weakened, the stiffness matrix will have to be modified and becomes a function of the current state of the structure and of its history. In

https://doi.org/10.1017/S0001924000010770 Published online by Cambridge University Press

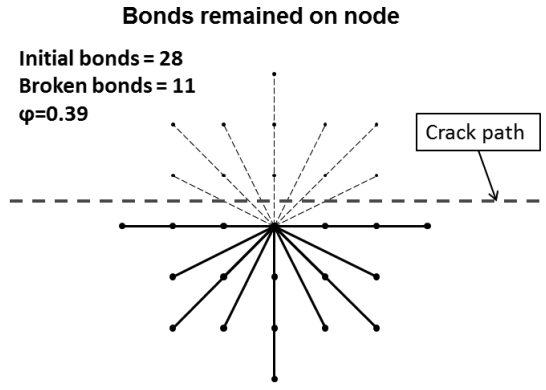


Figure 8. Damage index φ for a straight crack path which divides nodes within a horizon sphere.

this paper, a full N-R method is adopted (details about it are reported in appendix A) in order to update the stiffness matrix at each iteration.

4.0 STATIC EXAMPLES WITH CRACK PROPAGATION

Initially, the proposed static solution strategy has been applied to classic linear elastic cases and the obtained results have been compared to those obtained for the same problem solved with the finite element method (FEM) using the MsC.Nastran solver (in appendix B the relative results can be found) As pointed out in Ref. 27, we too found that the peridynamic analysis is able to capture the effective elastic behavior of the studied systems. The numerical accuracy of the results depends on the grid spacing: decreasing this parameter leads to an increase of the total number of nodes of the model and of the related computational cost. In this section peridynamic static solutions of crack propagation problems are compared to other solutions found in the scientific literature. The proposed solution approach has been investigated in two main phases: in the former, the dependence of the solution on the grid size (δ-convergence[28]) has been investigated, while in the latter the method has been used to study some reference cases for which the force versus displacement curves are presented and compared to published results.

4.1 Nonlinear solutions for varying grid size

The sensitivity study has been carried out on a symmetric double cantilever beam on which a controlled opening displacement is applied. The investigation varied the grid size Δx, but kept constant the m ratio between the radius δ and the grid size Δx (δ convergence, see Fig. 9).

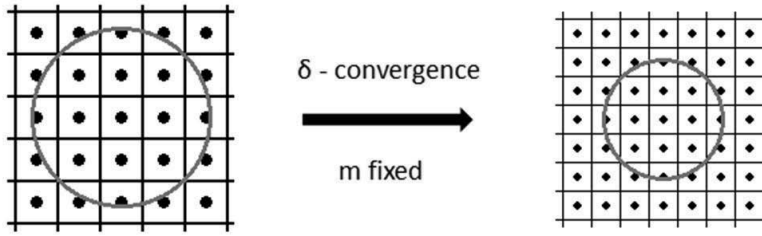
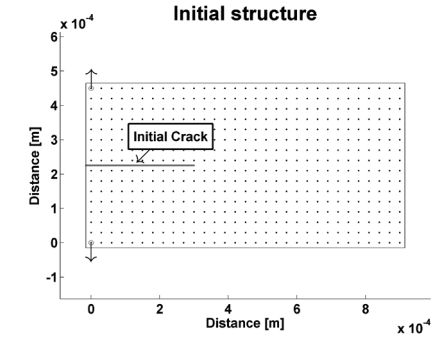


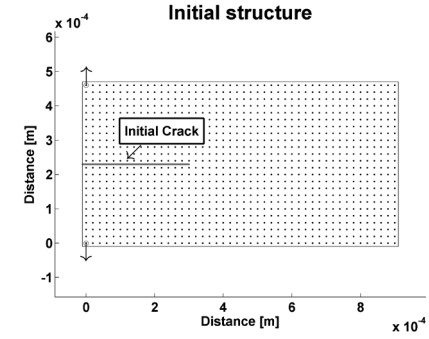
Figure 9. Example of δ -convergence, the grid size is reduced but the ratio $m = \delta/\Delta x$ is kept constant.

https://doi.org/10.1017/S0001924000010770 Published online by Cambridge University Press

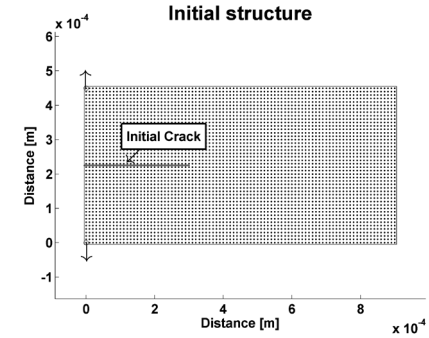
Three discretisation of the system under investigation are shown in Fig. 10. In all cases the opening displacement is imposed at the corner nodes, where the bonds are all linearly elastic, with no damage possibility. In this way no damage can affect the area where the displacement is directly imposed. The constitutive law of all other bonds is bilinear with the following properties (the bond stiffness c and the linear elastic limit stretch s_0 depend on the grid size Δx, according to Equation (6) and Equation (14)): $c = \frac{7 \cdot 6394 \cdot 10^9}{\Delta x^3}$ N/m^6, $s_0 = \sqrt{\frac{3 \cdot 2321 \cdot 10^{-11}}{\Delta x}}$ and $k_r = 1$ (it should be noted that for all the models the macro material parameters E and G_{Ic} are the same and equal to: $E = 72$GPa $G_{Ic} = 5$J/m^2). In all models the crack is introduced by removing the relevant bonds so that no bond is active between neighboring nodes which are separated by the crack, as shown in Fig. 5.



(a)



(b)



(c)

Figure 10. Double cantilever beam discretised with three different grid sizes: (a) Δx = 0·03mm; (b) Δx = 0·02mm; (c) Δx = 0·01mm.

https://doi.org/10.1017/S0001924000010770 Published online by Cambridge University Press

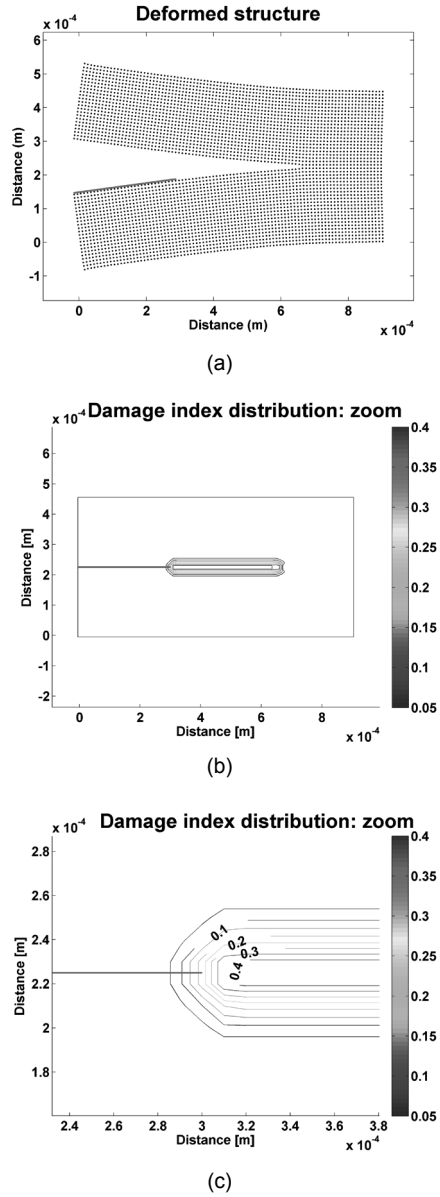


Figure 11. (a) Deformed shape, (b) damage index and (c) zoom of the damage index on the cracked area for the double cantilever system represented in Fig. 10 (all the displacements are magnified with a scale factor equal to 40).

The introduction of an initial notch is the only information provided to the model about the crack itself. An example of the results obtained with the most refined model (Δx = 0·01mm) is reported in Fig. 11.

The crack propagates from its initial length (a = 0·3mm) to the final length of 0·65mm, then the sudden and complete fracture of the specimen takes place. Fig. 12 shows the comparison between the load curves of the three models with increasing grid density.

https://doi.org/10.1017/S0001924000010770 Published online by Cambridge University Press

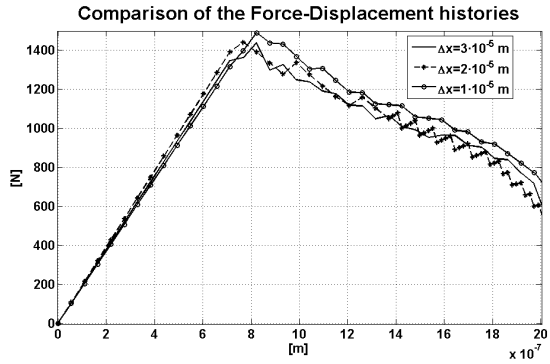


Figure 12. Applied external forces versus applied opening displacement for the three models with increasing grid density.

The results show that the overall slopes of the three load-displacement curves are very similar. In particular, the peak force (about 1,450N) and the external applied displacement at which it is reached ($8 \cdot 10^{-7}$m) are similar for all models.

4.2 Static solution of reference cases with peridynamic analysis

In the present section the static implementation of Peridynamics is used to reproduce several results previously published in scientific literature. Three cases are compared quantitatively and three only qualitatively since a comparison on numbers was not easy.

The required input parameters for the bilinear constitutive law are: δ, c, s_0 and s_c The horizon distance δ is chosen to be $3\Delta x$ as often done in the peridynamic literature[25]. The stiffness c is defined by means of Equation (6) and reproduces the elastic behavior of the material. The bond stretch s_0 marks the beginning of the nonlinear behavior and is evaluated from the analysis of load-displacement curve (see Refs 22 and 29): the point where the curve differs from linearity identifies the load condition at which the first bond in the peridynamic grid exceeds the linear limit. Finally the Equation (14) allows the evaluations of the ratio k_r and ultimately of the failure stretch s_c.

Using this approach, three examples have been simulated. Example 1 is taken from Ref. 29, where the geometric and material properties are defined, and it is shown in Fig. 13. The material

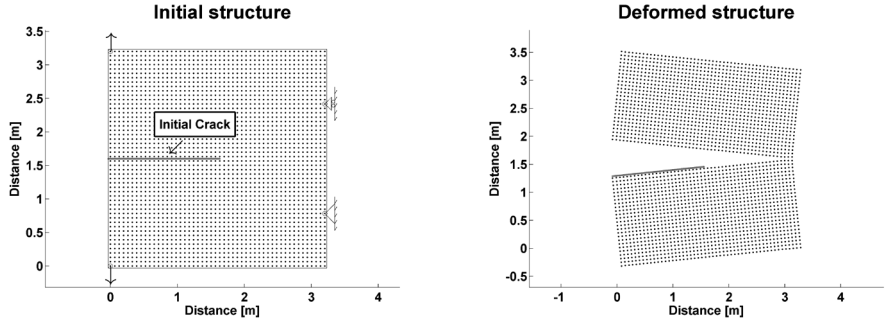


Figure 13. Double cantilever test on a pre-cracked plate (the geometry is the same as that seen in Ref. 29). (a) The system under study; (b) the deformed structure with the crack opening (a scale factor of 200 has been applied to all the displacements on this image).

https://doi.org/10.1017/S0001924000010770 Published online by Cambridge University Press

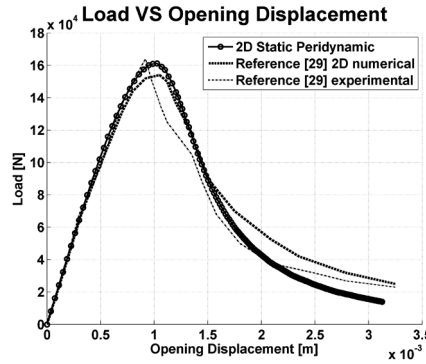


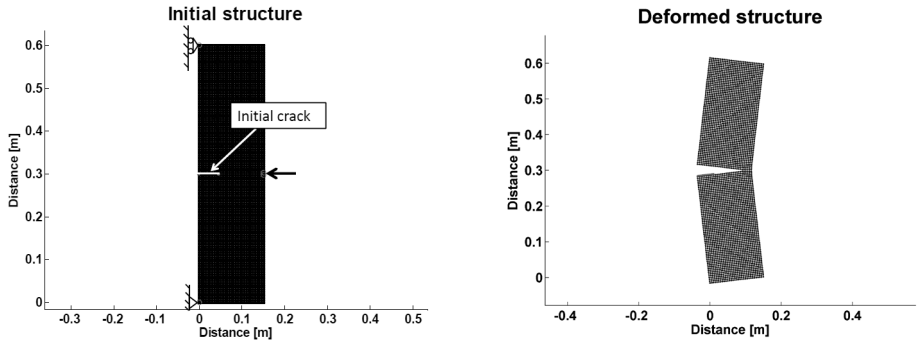
Figure 14. Comparison of the applied force versus the opening displacements obtained with static solution of the peridynamic problem and the results reported by X. Su[29].

parameters used to define the bilinear law are: the Young's modulus $E = 28{\cdot}3\text{GPa}$ and the fracture energy in mode I $G_{Ic} = 490\text{J/m}^2$. For the peridynamic analysis a grid size $\Delta x = 0{\cdot}0653\text{m}$ has been used so that a radius $\delta = 0{\cdot}1959\text{m}$ has been selected (m ratio = 3) for a total node number of 2,500. The bilinear bond force is characterised by the values: $c = 2{\cdot}6952{\cdot}10^{13}\text{N/m}^6$, $s_0 = 7{\cdot}8548{\cdot}10^{-5}$ and the ratio $k_r = s_c / s_0$ is equal to 20. The static solution of the peridynamic problem has been found using a controlled displacement method and the load-displacement curve of the applied external force versus the opening displacement is compared to the results of Ref. 29 in Fig. 14. The curve obtained with the peridynamic solver is in good agreement with the one obtained in Ref. 29 and with the experimental results. The static solution diagram follows the experimental results up the maximum force values (of about 160kN) then also the softening path is estimated in an acceptable way.

The second and third examples are three point bending tests as reported in Ref. 22: two cases have been studied where the only difference is the fracture energy of the material while all other geometric and mechanic parameters are unchanged and set equal to those used in Ref. 22.

The initial structure configuration, load and boundary conditions are shown in Fig. 15(a). Figure 15(b), on the other hand, represents the deformed configuration of the specimen at the end of the load history.

The two different values for the fracture energy G_{Ic} are $G_{Ic} = 9{\cdot}8\text{J/m}^2$ for example 2 and G_{Ic} 49J/m^2 for example 3. The solutions reported by Carpinteri[22] highlight as reducing only the fracture energy



(a) (b)

Figure 15. Three point bending test on a cracked plate (the geometry is equivalent to that reported in Ref 22). (a) system under study; (b) deformed structure with the crack opening (a scale factor of 600 has been applied to all the displacements on this image).

https://doi.org/10.1017/S0001924000010770 Published online by Cambridge University Press

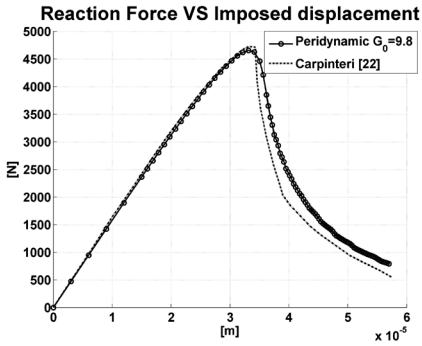


Figure 16. Load-displacement curve obtained for the three point bending test of a specimen with G_{Ic} = 9·8J/m^2.

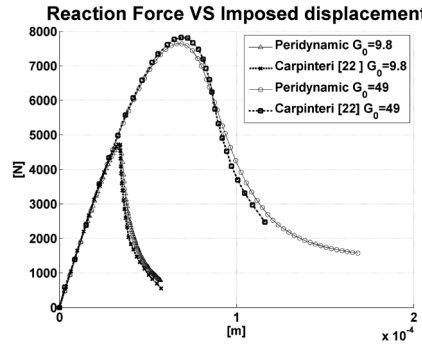


Figure 17. Comparison of the load-displacement curves obtained with various methods for the three point bending test of a specimen with G_{Ic} = 49J/m^2 and G_{Ic} = 9·8J/m^2.

values (and maintaining fixed the geometrical and the other material parameters) the softening branch of the force versus displacement curve becomes steeper with a sudden drop in the loading capacity. It is also shown that for some geometrical configuration a snap back behavior may occur.

The parameters used for these peridynamic analysis are E = 35·77GPa, Δx grid size of 0·005m, radius of 0·015m for a total node number of 3,720 in a plane stress static formulation. For the case with G_{Ic} = 9·8J/m^2, k_r is equal to 8·56 instead with G_{Ic} = 49J/m^2 k_r is 42·8, for both cases $c = 2{\cdot}0242{\cdot}10^{17}$N/m^6 and $s_0 = 5{\cdot}458{\cdot}10^{-5}$.

The results obtained with a fracture energy of 9·8J/m^2 are shown in Fig. 16; in the same figure the results published in Ref. 22 are reported.

Fig. 16 shows that the peridynamic solution is able to identify well the maximum value of the applied force and the displacement at which the load capability drops.

The shape of the softening part of the curve is correctly represented even if the residual load capability is over estimated.

Fig. 17 shows the results of the third example, the static solution obtained with the peridynamic theory with G_{Ic} = 49J/m^2. Also in this case the proposed method is able to correctly predict the peak force, the value of the corresponding displacement and the shape of the softening curve. In

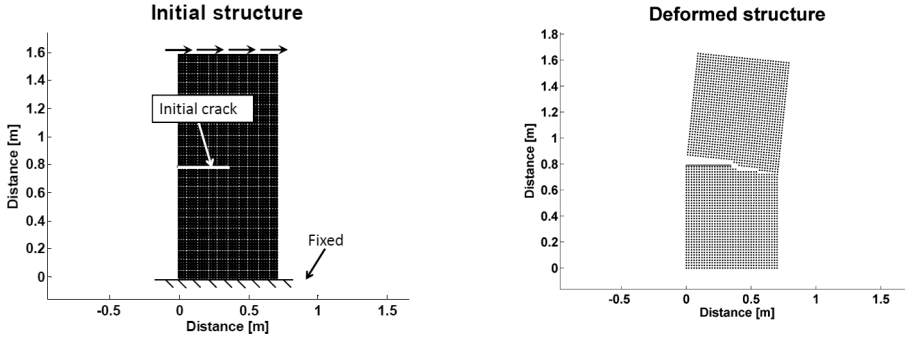


Figure 18. Cracked plate with external applied shear force: (a) the studied system, (b) the deformed structure with the crack opening (a scale factor equal to 280 has been applied to all the displacements on this image).

https://doi.org/10.1017/S0001924000010770 Published online by Cambridge University Press

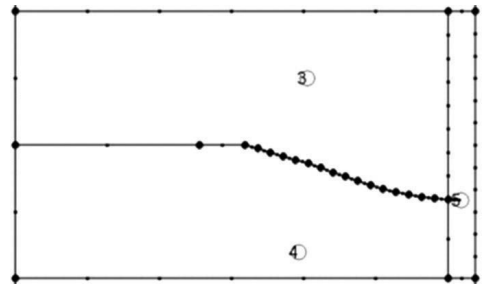


Figure 19. Crack shape in the plate with external applied shear force as reported[30], zoom in the crack area.

the same image the results of the previously described case with $G_{Ic} = 9{\cdot}8\text{J/m}^2$ are also shown. The area under the curves is related with the fracture energy. The proposed approach used to define the parameters for the bond force allows to correctly reproduce the results presented in Ref. 22 and underlines that it is possible to follow the sharp load reduction for the lower G_{Ic} values with a peridynamic analysis too.

The following computational examples present only a qualitative comparison between the peridynamic solutions and previously published results, in order to illustrate further the potentialities of the proposed method.

The comparison can only be qualitative due to lack of information in the published works or to the different nature of the performed analysis: for example one of the published solutions has been obtained using the crack tip advancement control method instead of applying a controlled external displacement. Moreover, in some cases the published results have been obtained using macro material parameters not supported by the bond-based peridynamic theory with particular reference to the value of Poisson's ratio.

Figure 18 shows a cracked plate to which a shear force is applied on an edge while the opposite edge is fixed. The geometrical and material parameters are width = 0·7m, height = 1·58m, E =30GPa, $G_{Ic} = 5\text{J/m}^2$; the static solution of peridynamic according to Ref. 30 has been evaluated assuming a plane strain condition; for this model the grid size Δx is 0·02m, the total number of nodes is 2,880 and the bilinear bond parameters are: $c = 4{\cdot}2441{\cdot}10^{14}\text{N/m}^6$, $s_0 = 1{\cdot}3484{\cdot}10^{-5}$ and $k_r = 20$. The last parameter (k_r) has been evaluated through a sensitivity analysis in order to reproduce

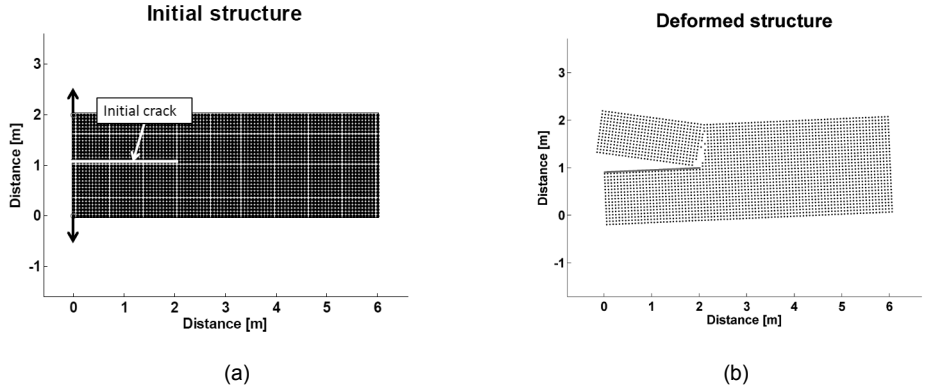
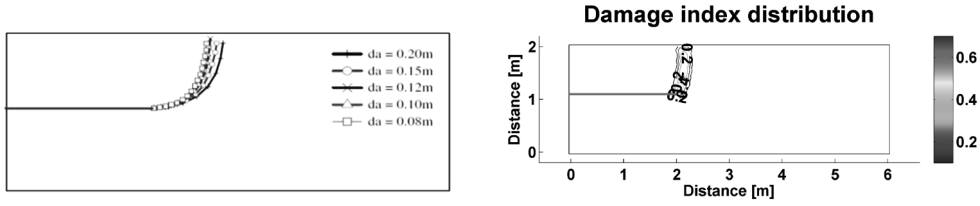


Figure 20. Double cantilever beam test with eccentric crack: (a) the studied system, (b) the deformed structure with the crack opening (a scale factor of 35 has been applied to all the displacements of this image).

https://doi.org/10.1017/S0001924000010770 Published online by Cambridge University Press



(a) (b)

Figure 21. Crack shape for eccentrically pre cracked plate: (a) the crack shape presented in Ref. 31 with some crack path obtained controlling increment on the crack tip advancement, (b) the damage index diagram obtained with the static analysis of the peridynamic problem.

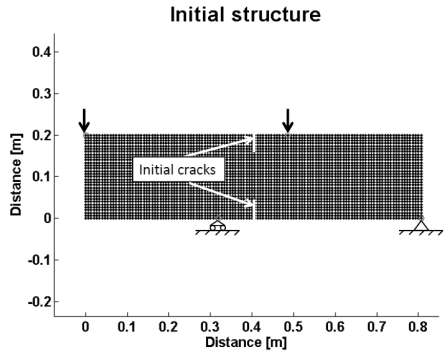
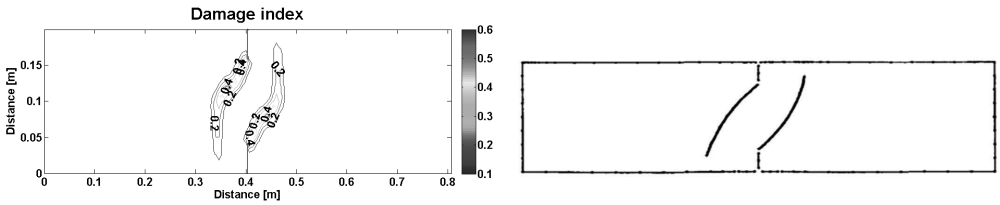


Figure 22. Double edge cracked plate under four point shear beam test.



(a) (b)

Figure 23. Double edge cracked plate under four point shear test: (a) the damage diagram obtained with static peridynamic solver, (b) the crack path reported in Ref. 32.

the crack shape. The peridynamic solution is able to correctly describe the shape of crack path in the case of mixed-mode crack propagation in this example too.

The results reported in Ref. 30 have been obtained performing a simulation where the external load is controlled by the crack tip advancement, whereas in the peridynamic approach an external horizontal displacement has been applied on the nodes of the top part of the structure, as shown in Fig. 18. Figure 19 shows the crack path obtained in Ref. 30.

Figure 20 shows a double cantilever beam with an eccentric crack; the material parameters are the same as reported on[31] ($E = 0{\cdot}1$MPa, $G_{Ic} = 0{\cdot}0015$J/m^2), as well as the specimen dimensions. For this analysis, a grid size with $\Delta x = 0{\cdot}0667$m has been used and the total number of nodes is 2,821. The bilinear bond parameters are: $c = 7{\cdot}1620{\cdot}10^7$N/m^6, $s_0 = 8{\cdot}6487{\cdot}10^{-5}$ and $k_r = 14$.

From the results of the static analysis, shown in Fig. 20(b) and Fig. 21(b), the crack path seems tortuous with respect to that found in Ref. 31 and reported in Fig. 21(a), however it should be noted

https://doi.org/10.1017/S0001924000010770 Published online by Cambridge University Press

that the peridynamic theory allows the crack propagation along the most convenient path from an energy view point without any additional constraint or assumption. Moreover the peridynamic solution has been obtained just by imposing the displacements of the corners of the plate, as shown in Fig. 20(a), whereas in Ref. 31 an incremental control on the crack advancement is applied.

As last example the static peridynamic solver has been applied to the case of four point shear beam test with double edge crack, as represented in Fig. 22; plane stress conditions have been considered. The system geometry and the material properties ($E = 27\text{GPa}$, $G_{Ic} = 100\text{J/m}^2$) have been selected according to Ref. 32. In this model the peridynamic grid size is $\Delta x = 0{\cdot}00667\text{m}$ and the total node number is 3,782. The bilinear bond law parameters are: $c = 4{\cdot}8343{\cdot}10^{17}\text{N/m}^6$, $s_0 = 1{\cdot}1370{\cdot}10^{-4}$ and $k_r = 20$. The results presented in Ref. 32 have been obtained assuming a Poisson's ratio for the material equal to $\nu = 0{\cdot}1$, whereas in the peridynamic case we are forced to have $\nu = 0{\cdot}25$.

The crack path obtained, visible from the damage diagram shown in Fig. 23(a), is compared to the one reported in Ref. 32 and shown in Fig. 23(b).

5.0 CONCLUSIONS

The peridynamic theory provides powerful tools to study the behavior of solid bodies with a non-local and mesh free approach. The theory is based on integral equations so that it is able to solve problems in presence of discontinuities (as cracks, voids, inclusions), moreover a clear concept of local damage is introduced. The paper presents the application of a peridynamic based computational method applied to static problems. An implicit Newton Raphson approach is adopted. Compared with computational techniques based on explicit dynamic relaxation[15], the proposed method is more computationally efficient and provides more control on the accuracy of the solutions.

The method has been applied to the study of nonlinear problems with quasi-static crack propagation for system under different load and boundary conditions. The static solution predicts crack paths similar to the ones obtained with different numerical approaches. Lastly, the comparison between the force versus displacement curves, whenever possible, showed a good agreement between the results predicted by the peridynamic static solution and the published results.

In the authors' opinion Peridynamics based computational methods constitute a very promising alternative to FEM in dealing with crack propagation. They could find useful application to problems in which damage evolution has to be closely followed and monitored with little or no a priori knowledge on the possible crack paths. Therefore Peridynamics based methods could be of the highest importance to describe damage processes affecting structural components in order to evaluate their life expectancy for a safe and economically sound utilisation.

ACKNOWLEDGEMENTS

The financial support of the University of Padova PRAT-CPDA111598 is gratefully acknowledged.

REFERENCES

1. ZEHNDER, A.T. *Fracture Mechanics, Series: Lecture Notes in Applied and Computational Mechanics*, **62**, Springer, London, UK, 2012.
2. MI, Y., CRISFIELD, M.A., DAVIES, G.A.O. and HELLWEG, H.B. Progressive delamination using interface elements, *J Compos Mater*, 1998, **32**, pp 1246-1272.

https://doi.org/10.1017/S0001924000010770 Published online by Cambridge University Press

3. MUNOZ, J.J., GALVANETTO, U. and ROBINSON, P. On the numerical simulation of fatigue driven delamination with interface elements, *Int J Fatigue*, 2006, **28**, pp 1136-1146.
4. TURON, A., DÁVILA, C.G., CAMANHO, P.P. and COSTA, J. An engineering solution for mesh size effects in the simulation of delamination using cohesive zone models, *Eng Fract Mech*, 2007, **74**, pp 1665-1682.
5. ZI, G. and BELYTSCHKO, T. New crack-tip elements for XFEM and applications to cohesive cracks, *Int J Numer Meth Eng*, 2003, **57**, pp 2221-2240.
6. BELYTSCHKO, T., CHEN, H., XU, J.X. and ZI, G. Dynamic crack propagation based on loss of hyperbolicity and a new discontinuous enrichment, *Int J Numer Meth Eng*, 2003, **58**, pp 1873-1905.
7. MÖES, N., STOLZ, C., CHEVAUGEON, N. and SALZMAN, A. The Thick Level Set Model: A non-local damage model allowing automatic crack placement inside localization zones, Proceedings of CFRAC 2013, Computational Modeling of Fracture and Failure of Materials and Structures, 5-7 June, Prague, Czech Republic, 2013.
8. NGUYEN, V.P., RABCZUK, T., BORDAS, S. and DUFLOT, M. Meshless methods: a review and computer implementation aspects, *Math Comput Simulat*, 2008, **79**, pp 763–813.
9. FLEMING, M., CHU, Y.A., MORAN, B. and BELYTSCHKO, T. Enriched element-free Galerkin methods for crack tip fields, *Int J Num Meth*, 1997, **40**, pp 1483–1504.
10. VENTURA, G., XU, J.X. and BELYTSCHKO, A. Vector level set method and new discontinuity approximations for crack growth by EFG, *Int J Num Meth Eng*, 2002, **54**, pp 923–944.
11. MUTHU, N., MAITI, S.K., FALZON, B.G. and GUIAMATSIA, I. A comparison of stress intensity factors obtained through crack closure integral and other approaches using eXtended element-free Galerkin method, *Comput Mech*, 2013, **52**, pp 587–605.
12. MUTHU, N., FALZON, B.G., MAITI, S.K. and HODDAM, S.K. Modified crack closure integral technique for extraction of SIFs in mesh free methods, *Finite Elementsin Analysis and Design*, 2014, **78**, pp 25-39.
13. SILLING, S.A. Reformulation of elasticity theory for discontinuities and long-range forces, *J Mech Phys Solids*, 2000, **48**, pp 175-209.
14. SILLING, S.A., WECKNER, O., ASKARI, E. and BOBARU, F. Crack nucleation in a peridynamic solid, *Int J Fract*, 2010, **162**, pp 219-227.
15. KILIC, B. and MADENCI, E. An adaptive dynamic relaxation method for quasi-static simulations using the peridynamic theory, *Theor Appl Fract Mech*, 2010, **53**, pp 194-204.
16. MITCHELL, J.A. A nonlocal, ordinary, state-based plasticity model for Peridynamics, Technical report, Sandia National Laboratories, SAND2011-3166, 2011.
17. MITCHELL, J.A. A non-local, ordinary-state-based viscoelasticity model for Peridynamics, Technical report, Sandia National Laboratories, SAND2011-8064, 2011.
18. PARKS, M.L., LITTLEWOOD, D.J., MITCHELL, J.A. and SILLING, S.A. Peridigm Users' Guide v1.0.0, Technical report, Sandia National Laboratories, SAND2012-7800, 2012.
19. LADANYI, G. and JENEI, I. Investigation of peridynamic plastic material model, Proceedings of the 4th IASME/WSEAS International Conference on Continuum Mechanics (CM'09), 2009.
20. BREITENFELD, M.S. *et al* Non-ordinary state-based peridynamic analysis of stationary crack problems, *Computer Meth in Appl Mech Eng*, 2014, **272**, pp 233-250.
21. LIU, W. and HONG, J.-W. A coupling approach of discretized peridynamics with finite element method, *Computer Meth in Appl Mech Eng*, 2012, **245-246**, pp 163-175.
22. CARPINTERI, A. and COLOMBO, G. Numerical analysis of catastrophic softening behavior (snap back instability), *Computer & Struct*, 1989, **31**, pp 607-636.
23. WARREN, T.L., SILLING, S.A., ASKARI, A., WECKNER, O., EPTON, M.A. and XU, J. A non-ordinary state-based peridynamic method to model solid material deformation and fracture, *Int J Solids Struct*, 2009, **46**, pp 1186–1195.
24. YU, K., XIN, X.J. and LEASE, K.B. A new method of adaptive integration with error control for bond-based peridynamics, Proceedings of the World Congress on Engineering and Computer Science Vol II – WCECS 2010, 20-22 October 2010, San Francisco, USA, 2010.
25. SILLING, S.A. and ASKARI, E. A meshfree method based on the peridynamic model of solid mechanics, *Computers & Struct*, 2005, **83**, pp 1526–1535.
26. CRISFIELD, M.A. *Non-Linear Finite Element Analysis Of Solids And Structures*, Wiley, Chichester, England, 1996.
27. SILLING, S.A. and LEHOUCQ, R.B. Convergence of peridynamics to classical elasticity theory, *J Elast*, 2008, **93**, pp 13–37.
28. HA, Y.D. and BOBARU, F. Studies of dynamic crack propagation and crack branching with peridynamics, *Int J Fract*, 2010, **162**, pp 229-244.

https://doi.org/10.1017/S0001924000010770 Published online by Cambridge University Press

29. SU, X. YANG, Z. and LIU, G. Finite element modeling of complex 3D static and dynamic crack propagation by embedding cohesive elements in Abaqus, *Acta Mechanica Solida Sinica*, 2010, **23**, pp 271-282.
30. YANG, Z. Fully automatic modeling of mixed-mode crack propagation using scaled boundary finite element method, *Eng Fract Mech*, 2006, **73**, pp 1711–1731.
31. ZHANG, H.H., LI, L.X., AN, X.M. and MA, G.W. Numerical analysis of 2D crack propagation problems using the numerical manifold method, *Eng Anal Bound Elem*, 2010, **34**, pp 41–50.
32. SALEH, A.L. and ALIABADI, M.H. Crack growth analysis in concrete using boundary element method, *Eng Fract Mech*, 1995, **51**, pp 533-545.

APPENDIX A

In this paper, a full N-R method is adopted in order to update the stiffness matrix at each iteration, since this method has a faster convergence than the modified version, where the tangent remains equal to the initial one at each iteration [26]. Using the conventional finite elements terminology, the equilibrium relationship between external and internal forces of the structure takes the following form:

$$[\mathbf{K}]\,\mathbf{u} = \mathbf{F} \qquad \ldots (A1)$$

where (**K**) is the global stiffness matrix of the structure, **u** is the vector of nodal displacements (containing two degrees of freedom per node, because of the two-dimensionality of the problem) and **F** is the external force vector. Since the problem is nonlinear, there is a direct dependence of the structure stiffness matrix on the displacement vector:

$$[\mathbf{K}] = [\mathbf{K}(\mathbf{u})] \qquad \ldots (A2)$$

The out of balance force vector **g** needs to be evaluated, in order to check if the force equilibrium is verified, namely if its values are all zero (within a given tolerance):

$$\mathbf{g} = \mathbf{F}_I - \mathbf{F}_E = [\mathbf{K}]\mathbf{u} - \mathbf{F} \qquad \ldots (A3)$$

If this function evaluated in $\mathbf{u} = \mathbf{u}_0$ is not the zero vector, according to the Newton-Raphson method[26], it is necessary to calculate the following derivative:

$$\frac{\partial \mathbf{g}}{\partial \mathbf{u}} = \frac{\partial}{\partial \mathbf{u}}\left([\mathbf{K}]\mathbf{u} - \mathbf{F}\right) = [\mathbf{K}] + \frac{\partial [\mathbf{K}]}{\partial \mathbf{u}}\mathbf{u} \qquad \ldots (A4)$$

The term $\left.\frac{\partial \mathbf{g}}{\partial \mathbf{u}}\right|_{\mathbf{u}=\mathbf{u}_0}$ represents the tangent to the curve $\mathbf{g} = \mathbf{g}(\mathbf{u})$ in the point $\mathbf{u} = \mathbf{u}_0$ and it is called tangent stiffness matrix $[\mathbf{K}]_T$. The following compact formula has been derived in order to express it:

$$k_{T_{ij}} = k_{ij} + \sum_{m=1}^{2n} \frac{\partial k_{im}}{\partial u_j} u_m \qquad \ldots (A5)$$

where i and j are the row and column suffixes respectively, and $2n$ is the total number of degrees of freedom (unknown displacements). Obviously, the contribution of a single bond to the tangent stiffness matrix $\left[\frac{\partial [\mathbf{K}]}{\partial \mathbf{u}}\mathbf{u}\right]_B$ is non-zero only for those bonds that have passed the linear elastic limit s_0, and that have a bilinear constitutive law (subscript B means that it refers to a single bond matrix). In the case of PMB, when the stretch exceeds the critical value s_c, the bond is removed from

https://doi.org/10.1017/S0001924000010770 Published online by Cambridge University Press

the system: accordingly, $\left[\frac{\partial[\mathbf{K}]}{\partial \mathbf{u}}\mathbf{u}\right]_B = 0$ for the bonds that still have a linear elastic behavior or that have a brittle constitutive law, therefore. $[\mathbf{K}]_{TB} = [\mathbf{K}]_B$ The global stiffness matrix is formed by assembling all bond contributions.

APPENDIX B

The proposed static solution strategy has been applied to three classic linear elastic cases, shown in Fig. B1, to verify and illustrate the performance of Peridynamics (PD) applied to linear problems.. The results of the static analysis have been compared to those obtained for the same problem solved with the finite element method (FEM) using the MsC.Nastran solver.



Figure B1. case 1, cantilever beam with tip force; case 2, cantilever beam with tip moment; case 3, simply supported beam with uniformly distributed load.

The results obtained with the static solution of Peridynamics have been reported in Fig. B2, Fig. B3 and Fig. B4 together with the relevant results obtained with finite element method: the comparison was made between peridynamic and FEM model both with 20 × 400 nodes.

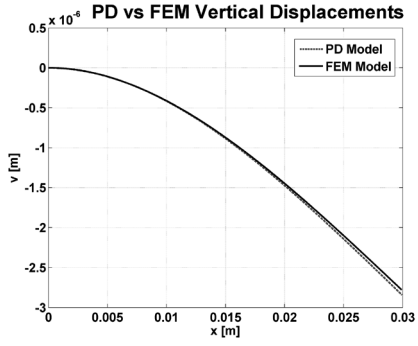


Figure B2. Case 1 of Fig. B1: comparison between Peridynamics and FEM results. *v* is the vertical displacement of the axis of the beam.

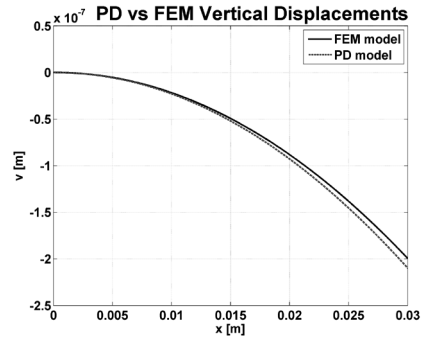


Figure B3. Case 2 of Fig. B1: comparison between Peridynamics and FEM results. *v* is the vertical displacement of the axis of the beam.

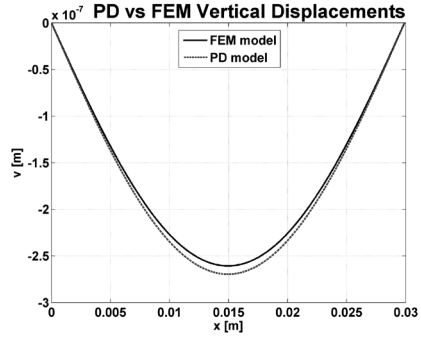


Figure B4. Case 3 of Fig. B1: comparison between Peridynamics and FEM results. *v* is the vertical displacement of the axis of the beam.

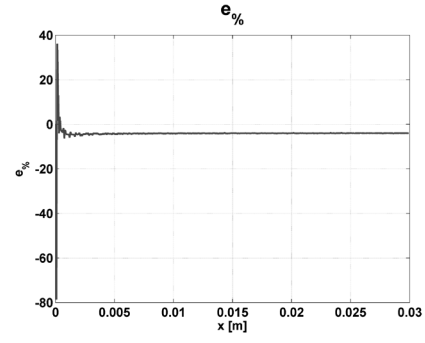


Figure B5. Case1: relative error of peridynamic solution respect to FEM solution. Vertical displacement of the nodes of the axis of the beam.

https://doi.org/10.1017/S0001924000010770 Published online by Cambridge University Press

Fig. B5, Fig. B6 and Fig. B7 show the relative error of the peridynamic solution with respect to that obtained with FEM.

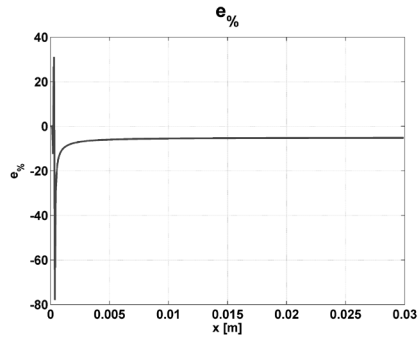


Figure B6. Case 2: relative error of peridynamic solution respect to FEM solution. Vertical displacement of the nodes of the axis of the beam.

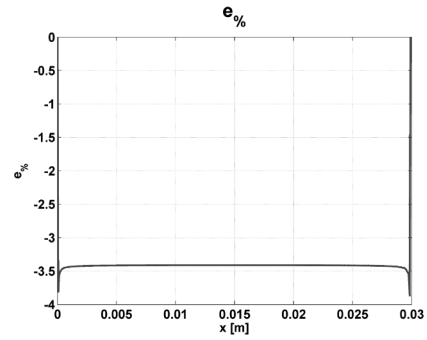


Figure B7. Case 3: relative error of peridynamic solution respect to FEM solution. Vertical displacement of the nodes of the axis of the beam.

The peridynamic solution is overall accurate except in the zone of the structure where the boundary conditions are applied, where displacements are very small. If we disregard those zones the maximum error for case 1 is about 2·3%, for case 2 is about 5·5% and for case 3 the maximum relative error is less than 3·5%.

The observed error where the boundary conditions are applied is due to the way the peridynamic theory deals with external loads and constraints[13,25]: they are applied within a horizon distance. The error along the span of the beam is due as well to the skin softening effect[25] related to the material points that are less than one horizon away from the system edges: this effect can be controlled by reducing the grid size Δx.

The relative error depends, in fact, on the grid size as shown Fig. B8, where the relative error of the tip displacement for case 1 is shown as a function of the uniform grid size Δx. The studied peridynamic models have the dimensions given in Table B1:

Table B1
Grid sizes and numbers of nodes along *x* and *y* directions used in the sensitivity analysis

Δx (m)	n_x	n_y
$0{\cdot}3{\cdot}10^{-4}$	100	5
$0{\cdot}15{\cdot}10^{-4}$	200	10
$0{\cdot}1{\cdot}10^{-4}$	300	15
$0{\cdot}075{\cdot}10^{-4}$	400	20

https://doi.org/10.1017/S0001924000010770 Published online by Cambridge University Press

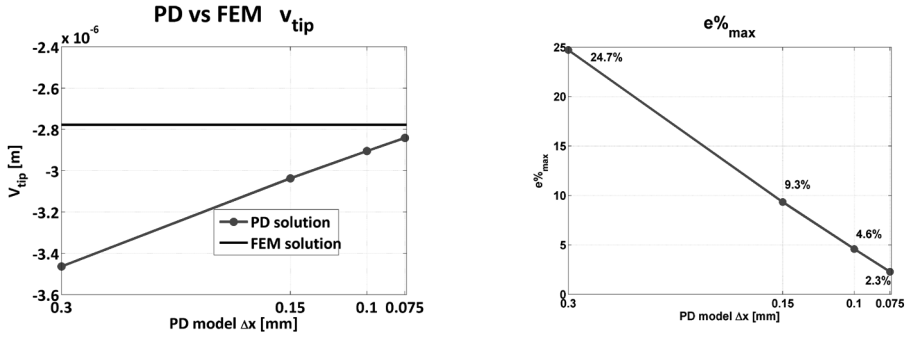


Figure B8. On the right image is shown the relative error for the tip displacement of case 1 versus the peridynamic grid size. On the left image is shown the PD tip displacement versus the FEM results.

The proposed static approach for the peridynamic analysis is able to capture the effective elastic behavior of the studied systems. The numerical accuracy of the results depends on the grid spacing decreasing this parameter means increasing the total number of nodes of the model. It should be also pointed out that a large number of nodes reduces the skin softening effect and allows for a better comparison between the boundary conditions of the peridynamic models and those of the finite element models.

https://doi.org/10.1017/S0001924000010770 Published online by Cambridge University Press